



UNIVERSITY OF LEEDS

This is a repository copy of *Numerical Simulation of Surface Subsidence After the Collapse of a Mine*.

White Rose Research Online URL for this paper:
<http://eprints.whiterose.ac.uk/172336/>

Version: Accepted Version

Proceedings Paper:

Derbin, YG, Walker, J, Wanatowski, D orcid.org/0000-0002-5809-0374 et al. (1 more author) (2019) Numerical Simulation of Surface Subsidence After the Collapse of a Mine. In: Sustainable Civil Infrastructures. The GeoChina 2018 International Conference, 23-25 Jul 2018, HangZhou, China. Springer International Publishing , pp. 80-97. ISBN 9783319956442

https://doi.org/10.1007/978-3-319-95645-9_9

© Springer International Publishing AG, part of Springer Nature 2019. This is an author produced version of an article published in Sustainable Civil Infrastructures. Uploaded in accordance with the publisher's self-archiving policy.

Reuse

Items deposited in White Rose Research Online are protected by copyright, with all rights reserved unless indicated otherwise. They may be downloaded and/or printed for private study, or other acts as permitted by national copyright laws. The publisher or other rights holders may allow further reproduction and re-use of the full text version. This is indicated by the licence information on the White Rose Research Online record for the item.

Takedown

If you consider content in White Rose Research Online to be in breach of UK law, please notify us by emailing eprints@whiterose.ac.uk including the URL of the record and the reason for the withdrawal request.



eprints@whiterose.ac.uk
<https://eprints.whiterose.ac.uk/>

NUMERICAL SIMULATION OF SURFACE SUBSIDENCE AFTER THE COLLAPSE OF A MINE

Y. G. Derbin^{1,2*}, J. Walker^{1,2}, D. Wanatowski^{2,3}, and A. M. Marshall⁴

¹ University of Nottingham, Ningbo, China

² State Key Laboratory for GeoMechanics and Deep Underground Engineering, China University of Mining & Technology, China

³ University of Leeds, Leeds, United Kingdom

⁴ University of Nottingham, Nottingham, United Kingdom

* Yury.Derbin@nottingham.edu.cn

ABSTRACT: Surface subsidence is a concern for many underground mining activities. If not predicted, this phenomenon can cause severe infrastructure damage. In this paper, a computer model is used to predict surface subsidence after the controlled collapse of a coal mine at Naburn in North Yorkshire, England. Scarcity of data on the characteristics of deep underground distressed and caved zones around coal mining excavations makes the numerical prediction of mining-induced subsidence very difficult. The authors derive appropriate input parameters for the numerical model using available borehole data with all necessary justifications provided. Simulations are performed using the commercial software FLAC3D. Different constitutive models, such as Mohr-Coulomb, modified Hoek-Brown, strain-softening, double yield, and modified Cam-clay are used to obtain surface subsidence profiles, which are compared against measurements taken at the site. Special attention is given to numerically simulating processes involved in the underground movements. It is shown that none of the models listed above can reasonably predict the surface subsidence profile.

Keywords: coal mining, numerical modelling, surface subsidence, caved zone, distressed zone

1. INTRODUCTION

Any underground work can cause surface subsidence, which could damage infrastructure and buildings. Longwall coal mining is not an exception. In order to mitigate consequences of the subsidence and choose the appropriate method of mining, it is important to predict the size and depth of the trough. Some empirical methods of surface subsidence prediction have been developed in different countries based on the observed local data; for example, one of them is in the Subsidence Engineers' Handbook (NCB, 1975) developed in the UK. FLAC3D is commercial software, which has been used to predict the surface subsidence trough (Herrero et al., 2012 and Xu et al., 2013). However, due to the complex behaviour of the rock, there is minimal confidence in predictions from numerical modelling and more research is required (Xu et al., 2013). The purpose of this work is to increase the understanding and develop the procedure of the numerical simulation of the surface subsidence with limited information on the properties of the overburden.

The following procedure are followed:

-Deriving model parameters from the borehole data;

- Setting the domain of the model;
- Assigning the constitutive model;
- Assigning the parameters derived earlier;
- Setting initial and boundary conditions;
- Running the model to equilibrium;
- Assigning the special constitutive model to the excavating zone to model goaf behavior;
- Assigning the parameters, which are inherited from the roof layer or derived from the literature, to the goaf;
- Assigning characteristics of the volumetric behavior of the goaf;
- Running the model to equilibrium;
- Altering volumetric characteristics in the goaf to obtain the required goaf height after the simulation (adjusting the goaf height).

The paper explains the procedure and discusses the modelling results in three parts. The first part explains a method developed by the authors for estimating and assigning the appropriate physical-mechanical properties to the model using a visual description of the borehole log. This method was created after an extensive literature search and based on the works of Balmer (1952), Deere (1968), Hoek and Brown (1980), Hansen (1988), Palmström (1995), Hoek and Brown (1997), Palmström and Singh (2001), and Hoek and Diederichs (2006). The second part describes the site of interest, the model domain, the mesh density, the initial and boundary conditions. The site is at Naburn in North Yorkshire, England. A measured subsidence profile was obtained from UKCoal. The mine collapsed uncontrollably after Longwall mining without stowing. The third part discusses results, the modelled stresses in the goaf, the debris caused by a mine collapse, the influence of the Geological Strength Index (GSI) and surface subsidence.

2. PHYSICAL-MECHANICAL PROPERTIES

2.1 Elastic Stiffness

Before developing a surface subsidence model, the estimation of the strength and deformation characteristics of rock masses should be carried out. It can be done in the laboratory, but it is expensive and suitable samples are not always available. After a wide literature review, a method for the estimation of the rock properties based on the borehole log description was developed and is presented in this section.

A key property of the material is the elastic stiffness. Hoek and Diederichs (2006) estimated it by the formula

$$E = E_i \left(0.02 + \frac{1 - D/2}{1 + e^{(60 + 25D - GSI)/11}} \right) \quad (1)$$

where GSI is the Geological Strength Index introduced by Hoek and Brown (1997) and describes the insitu state of the rock. A GSI of 100 is for a very good, undisturbed rock mass whereas a GSI of 0 is for a very poor quality, disintegrated rock mass. D is the disturbance factor, which is dependent upon the excavation conditions, i.e. blasting a

rock face will give the rock a disturbance factor of 1 while careful excavation will yield a disturbance factor of 0. E_i is given by:

$$E_i = MR \cdot \sigma_{ci} \quad (2)$$

where MR is the modulus ratio classified by rock type and presented in Table 1, MR was first proposed by Deere (1968) and later modified by Palmström and Singh (2001). σ_{ci} is the uniaxial compressive strength of the intact rock, which could be found in Table 2.

2.2 Failure Parameters

Hansen (1988) and Hoek and Brown (1980) developed the algorithm to determine failure parameters based upon a description of a borehole log. In order to find the Mohr-Coulomb parameters, cohesion and internal friction, the Hoek-Brown failure criterion is approximated with a Mohr-Coulomb failure surface by following the work of Hoek and Brown (1997). Equation 3, the Hoek-Brown empirical failure criterion for jointed rock masses, provides values of σ_1 that lay on the yield surface for different values of σ_3 hence it can be used to generate the maximum and minimum principal stresses for the rock in question.

$$\sigma_1' = \sigma_3' + \sigma_{ci} \left(m_b \frac{\sigma_3'}{\sigma_{ci}} + s \right)^{0.5} \quad (3)$$

Correspondingly, the values of m_b , and s in Equation 3 are given by:

$$m_b = m_i \cdot \exp\left(\frac{GSI - 100}{28}\right) \quad \text{if } GSI > 25 \quad (4)$$

where, m_i refers to the value of m for intact rock in the Hoek-Brown model and is summarized in Table 3, and

$$s = \exp\left(\frac{GSI - 100}{9}\right) \quad (5)$$

Then, the values for σ_3 must be selected. Hoek & Brown (1997) concluded that the most consistent results are obtained when 8 equally spaced values between $0 < \sigma_3 < 0.25\sigma_{ci}$ are used.

To find the tangent of the failure surface at the appropriate stress level, first the non-linear analytical solution for Mohr's envelope is found and then a linear regression analysis is used to find the equation of the tangent at that point.

Balmer's analytical solution (Balmer, 1952) to Mohr's envelope describes the relationship between the normal and shear stresses in terms of the principal stresses as:

$$\sigma_n' = \sigma_3' + \frac{\sigma_1' - \sigma_3'}{\frac{\partial \sigma_1'}{\partial \sigma_3'} + 1} \quad (6)$$

$$\tau = (\sigma_1' - \sigma_3') \sqrt{\frac{\partial \sigma_1'}{\partial \sigma_3'}} \quad (7)$$

Provided that the GSI is greater than 25 we can calculate

$$\frac{\partial \sigma_1'}{\partial \sigma_3'} = 1 + \frac{m_b \sigma_{ci}}{2(\sigma_1' - \sigma_3')} \quad (8)$$

The tensile strength of the rock is calculated by substitution of $\sigma_1 = 0$ and $\sigma_{tm} = -\sigma_3$ in the Hoek-Brown failure criterion (Equation 3):

$$\sigma_{tm} = \frac{\sigma_{ci}}{2} \left(m_b - \sqrt{m_b^2 + 4s} \right) \quad (9)$$

The equivalent Mohr envelope may be written as:

$$Y = \log(A) + B \cdot X \quad (10)$$

which requires determination of A and B. The values of X and Y can be calculated using Equations 7, 8, and:

$$Y = \log\left(\frac{\tau}{\sigma_{ci}}\right) \quad (11)$$

$$X = \log\left(\frac{\sigma_n' - \sigma_{tm}}{\sigma_{ci}}\right) \quad (12)$$

The constants A and B can then be calculated using a linear regression analysis, i.e.

$$A = 10^{\left(\frac{\sum Y/T - B(\sum X/T)}{\sum Y/T - B(\sum X/T)}\right)} \quad (13)$$

$$B = \frac{\sum X \cdot Y - (\sum X \cdot \sum Y)/T}{\sum X^2 - (\sum X^2)/T} \quad (14)$$

where T is the number of values in the sequence, i.e. 8, if the earlier suggestion is followed.

Finally, the Mohr-Coulomb parameters can be deduced from the following two equations:

$$\phi = \tan^{-1} \left(A \cdot B \cdot \left(\frac{\sigma_{ni}' - \sigma_{tm}}{\sigma_{ci}} \right)^{B-1} \right) \quad (15)$$

$$c = 0.75 \left(\tau - \sigma_{ni}' \tan(\phi) \right) \quad (16)$$

Since A and B are known, then using σ_{ni} in place of σ_n , (i.e. general notation of the normal stress), in Equation 12 will evaluate an expression for X which can be used in Equation 10 to find a value of Y. This can be used to calculate τ from Equation 11.

It can be seen that another new parameter (σ_{ni}) has been introduced and this is the value of the normal stress at the point of interest. To determine this value we need to turn to the work of Hoek and Brown (1980).

Hoek and Brown found the correlation (Eq. 17) between depth and vertical insitu stress based on the collated worldwide data from researchers investigating the insitu state of stress underground (Figure 1).

$$\sigma_{ni} = 0.027 \cdot z \quad (17)$$

The vertical stress calculated by Equation 17 is given in MPa. This value is equivalent to the normal stress and enables us to completely specify the mechanical properties of the rocks underground.

3. MODEL DEVELOPMENT

3.1 Site of Interest

A measured subsidence profile and the borehole log description were taken from both above and under the Barnsley seam at Naburn in North Yorkshire, UK. The overburden consists of siltstone, sandstone, mudstone, and seatearth (claystone underlying coal seam). The bulk and shear moduli were calculated using Equations 1 and 2 for the elastic stiffness and assuming a Poisson's ratio of 0.2 for all layers. The internal friction and cohesion were derived from Equations 15 and 16. The tensile strength was calculated by Equation 9. A density of 2700 kg/m³ was taken as an average value for these types of rock after data collected by Shtumpf (1994) in Table 4.

3.2 Model Domain

Due to the symmetry of the problem, the model domain could be reduced by half of the profile to reduce running time of the simulation. The size of domain was chosen in such a way that the boundary conditions did not impact on the result. Figure 2 shows the sizes of the model, the placement of the goaf, the location of the roller boundary conditions, and two different densities of the mesh. The excavation under investigation was 2.8m thick, 75m wide, and 709.6m below the surface. The model was fixed in the out of plane direction. The bottom of the model was fixed in the vertical direction, and two sides were fixed in the horizontal direction. The lowest density mesh was located where the stresses were low following the recommendations of the FLAC3D manual (Itasca, 2013). Either the Mohr-Coulomb, modified Hoek-Brown, or the strain-hardening/softening models constituted the behaviour of the whole subsurface. The exception was the goaf material, where the double yield and later the modified Cam-clay models were implemented.

3.3 Simulation of the Goaf Behaviour

According to Najafi et al (2014), the simulation of the goaf behaviour is important for the accuracy of the subsidence prediction. Herewith, the goaf material is deep underground and it is difficult to estimate its properties. There have been numerous attempts at characterizing the goaf behaviour in the literature. For example, Salamon (1983) described the volumetric compression properties of the goaf material by the following equation:

$$\sigma = \frac{\alpha \varepsilon}{\beta - \varepsilon} \quad (18)$$

where α and β are empirical constants.

Later, Salamon (1990) rewrote Equation 18 and eliminated the empirical constants by using certain physical parameters.

$$\sigma = \frac{E_0 \varepsilon}{(1 - \varepsilon / \varepsilon_m)} \quad (19)$$

where E_0 is the initial tangent modulus and ε_m is the maximum strain of the goaf material.

Since the parameters are difficult to estimate, and even sometimes impossible, the authors of this paper go further with assumptions. Equation 18 can be rewritten considering the coefficient $\gamma=1/\varepsilon_m$, which is used to adjust the height of the goaf after a simulation, and E is the Young's modulus of the roof material.

$$\sigma = \frac{E\varepsilon}{(1-\gamma\varepsilon)} \quad (20)$$

The correctness of the modelled goaf behaviour is possible to check by two facts: the goaf height and the stresses in the goaf after the simulation. The stresses in the goaf will be discussed in the next section.

The required goaf height at the end of the simulation can be estimated by the initial height of the seam. The required height can be found by the multiplication between the height of the mine and the subsidence factor: these are collected in Table 5 for different regions of the world by Bräuner (in Bell and Donnelly, 2006). The subsidence factor depends on the region and whether or not the excavated area has been filled or packed. The factor is used to calculate maximum possible subsidence. Table 5 shows the subsidence factor varies from 0.33 to 0.9 for the different regions. The recommended factor is 0.9 for mines in UK. For the case at hand with a height of the excavation of 2.8m, the required final height of the goaf is estimated as 0.28m. Altering the parameter γ , the simulation was repeated until the goaf height after the simulation becomes within 5% error of the required height. For the sake of simplicity, this process of obtaining the required goaf height by altering the volumetric characteristics of the goaf is called 'adjusting goaf height'.

In order to model the strain-hardening behaviour of the goaf material, the double yield model, which allows both shear and volumetric compression, is traditionally implemented. In FLAC, the stress-strain curve is approximated by a table to generate a linear piecewise curve. In the developed model, the table has 10 rows. The elastic properties, bulk and shear moduli, and Mohr-Coulomb properties, friction and cohesion, correspond to the properties of the roof material.

As it will be shown later, the double yield model cannot simulate the goaf behaviour precisely enough. Instead, one of the Critical State models, namely the modified Cam-clay model, was implemented. Derbin et al. (2016) showed that the modified Cam-clay model predicts the goaf behaviour more accurately than the double yield model. Computational application of Critical State theory includes different types of soil and soft rock (Gens, and Potts, 1988). Xiao et al. (2016) successfully implemented the Critical State concept to predict the behaviour of coarse granular soil (which is a material suitable for a rockfill dam) in a true triaxial compression test. The rockfill could best be described as a very coarse granular type of soil according to the British Soil Classification System (BS 5930:1981). The very coarse soils are cobbles with sizes of 63-200mm, boulders with sizes of 200 - 630mm, and large boulders with sizes of more the 630mm. Singh and Singh (2011) argued that goaf consists of 22.5% boulders and

77.5% large boulders. It should be also noted that the elastic properties depend on strain in the modified Cam-clay model. This corresponds better to the real behaviour of the goaf (Badr et al., 2003).

The goaf material was described by critical state parameters, i.e. $\lambda=0.188$, $\kappa=0.007$ and a frictional constant $(M)=1.9$, which were used by Indraratna and Salim (2002) to model drain triaxial shearing on crushed basalt. By changing either the specific volume at reference pressure on the normal consolidation line or the pre-consolidation pressure, the required height of the goaf can be obtained. Figure 3 shows curves of dependence between the obtained goaf height and specific volume for three different pre-consolidation pressures, i.e. 1e5Pa, 1e4Pa, and 1e3Pa.

4. MODEL RESULTS

4.1 Surface Subsidence

The existing constitutive models that are available in almost all commercial software aren't capable of providing accurate solutions. Figures 4a and 4b depict the surface settlement half-profiles. The distance zero corresponds to the centre line of the excavation, and it is assumed that there is little or no gradient across the longwall face so that the subsidence profile is symmetrical about the excavation's centreline. In Figures 4a and 4b, it can be noticed that the empirical method provided by the Subsidence Engineers' Handbook (NCB, 1975) fails to predict the correct depth of the trough, but it does predict the spatial extent very well. The results of the Mohr-Coulomb and Hoek-Brown failure criteria fail to predict both the depth and the spatial extent, but the results of both models agree closely with each other. This agreement means that the method of the calculation of the Mohr-Coulomb properties from the Hoek-Brown parameters is correct.

Further investigation includes the implementation of the strain-softening model. The model uses the Mohr-Coulomb failure criterion to detect failure and the cohesion of the rocks will suffer a post failure reduction in strength. Using test results, Pourhosseini and Shabanimashcool, (2014) proved that the post failure friction angle is constant. For post-peak variations of inherent cohesion, Pourhosseini and Shabanimashcool (2014) suggested a function:

$$c = c_0 \left(1 - \frac{\tanh(100\gamma_p)}{\tanh(10)} + 0.001 \right)^n \quad (21)$$

where γ_p is the plastic shear strain, %; c_0 is the cohesion at the peak strength of the rock where $\gamma_p=0$, and n is the fitting parameter, which depends on rock type and its magnitude varies from 0.29 for Sandstone to 0.34 for Mudstone (Pourhosseini and Shabanimashcool, 2014). After the evaluation of the effect of this parameter on the subsidence profile, no effect was noticed after the goaf height was adjusted. A mean value of 0.3 was taken in this work.

Figure 4a demonstrates that the strain-softening constitutive model predicts an identical subsidence profile to those profiles obtained by the Mohr-Coulomb and Hoek-Brown

models. However, the earlier investigations (i.e. by Lloyd et al, 1997) showed that the strain-softening model is capable of predicting a deeper trough than the Mohr-Coulomb model. This can be explained by examining the zone of plasticity. Figure 5a shows that the area of plastic deformation occurs directly above and under the excavation. After adjusting the goaf height, the strain-softening model shows the identical results as the Mohr-Coulomb model.

4.2 Geological Strength Index

The choice of the GSI influences where the plastic deformations occur (above or under the goaf). As it was mentioned before, the GSI stands for Geological Strength Index, a system of rock-mass characterization. Practically, the GSI should increase with the depth because the deeper geomaterial is, the less weathered and in better condition it is. If the GSI increases with the depth, the failure area above the goaf appears abundant. To show this, the GSI was increased by 2 each under- and overburden layer from 25 to 85 from the surface to the bottom of the model as shown in Figure 6a. The under- and overburden at hand is of multiple rock types including, mudstone, sandstone, seatearth, and siltstone (which is the roof material). The layers are too thin to be clearly shown on the diagram (Figure 6). Figure 6a shows the constant GSI and the increasing GSI with the depth. Figure 6b presents the diagram of the stiffness, which is calculated according to Equation 1 vs depth for two cases: when the GSI is constant and when the GSI changes from 25 to 85 with the depth according to Figure 6a. In Figure 5b, it can be seen that the model with the increasing GSI experiences more plastic deformation above the seam than the model with the constant GSI (Figure 5a).

The plastic zone distribution influences the performance of the strain-softening model. In contrast to the model with the constant GSI (Figure 4a), Figures 4b shows that the strain-softening model with the increasing GSI predicts a deeper trough than the Mohr-Coulomb model; however, this trough predicts an erroneous width if it is compared to the field measurements. More research on computer modelling of the surface subsidence is needed.

4.3 Stresses in the Goaf

Based on earlier research, Derbin et al. (2016) concluded that the vertical stresses in the goaf after perturbation should recover to the natural stresses at some sufficient distance from the goaf rib; however, during the current simulation, it was noticed that this did not occur. Figure 7a presents both the theoretical stress distribution at a depth equal to the roof of the seam and several key characteristics, which help describe the stress arrangements after the collapse of a mine. They are three distances D1, D2, and D3; D1 is the distance into the goaf from the goaf rib where the stresses recover to the primary stress, D2 is the distance between the lowest residual stress in the goaf and the insitu stress in the unexcavated seam and D3 is the distance between the lowest stress in the goaf and the highest (peak) induced stress on the seam rib. D3 appears due to coal crushing at the seam rib, and it can be minimal or absent if crushing is not significant.

In order to investigate stress recovery in the goaf, Derbin et al. (2016) developed a simplified fictitious subsidence model where the goaf length is equal to distance D1. Distance D1 was calculated using the following equation suggested by Mukherjee (1994) (after Wilson, 1984):

$$D1 = 0.3-0.4 \cdot H \quad (22)$$

where H = the thickness of the overburden.

The traditional double yield model and the modified Cam-clay model were implemented to represent goaf material behaviour. Figure 7b shows that both models predict stresses of 6MPa, which is lower than the primary stresses (10.5MPa). It means that the both models fail to predict the correct behaviour of the goaf. At the same time, if Figure 7a and Figure 7b are collated, it can be noticed that the results obtained with the help of the modified Cam-clay model are closer to the theoretical expectations. The peak and lowest stresses predicted by the modified Cam-clay model are higher and lower respectively than the stresses predicted by the double yield model. It means the modified Cam-clay model is better at predicting the behaviour of the goaf material.

Contrary to the research described above, where the goaf length is sufficient for recovering the primary stress, the goaf length is only 75m in this research, which is more than three times less than necessary for the reestablishment of the primary stress. In the model for the Naburn site, H is 706.8m, therefore following Equation 22, D1 should be approximately 250m. As a result, Figure 8 shows that the stress in the goaf of the subsidence profiles obtained using the double yield model and modified Cam-clay for the Naburn site are identical.

5. CONCLUSIONS

The paper describes how to simulate surface subsidence after a goaf collapse for any seam in any part of the world using only the description of the borehole log. The method of calculation of the Mohr-Coulomb properties out of the Hoek-Brown parameters was introduced. The predictions of the Mohr-Coulomb and modified Hoek-Brown constitutive models embedded in FLAC agree with each other. This proves the correctness of the method used to calculate the properties. The strain-softening method predicts identical deformation, magnitude, and spatial extent for a constant GSI, but the variable GSI causes a deeper trough.

A pattern of plastic deformation around the goaf is crucial for the strain-softening model. When plastic deformation above and under the goaf is in the same quantity, the strain-softening effect of the model is compensated by adjusting the goaf height. All these plastic zones act as one big goaf. The pattern of plastic deformation depends on relationship between the GSI and depth. The GSI increasing with the depth produces a larger failure area above the goaf, which deepens the trough of the strain-softening model. Unfortunately, this is not sufficient to match field observations in this research, and the trough keeps the same erroneous width. Hence, practitioners should use traditional constitutive models to predict surface subsidence with great care.

For the time being, the best solution would be utilization of the strain-softening

constitutive model keeping in mind that it can underestimate the depth and overestimate the width of the subsidence trough. To improve the prediction of the sizes of the trough, more advanced constitutive models should be implemented. The recent research by Derbin et al. (2018) has shown that the bubble model has better results. It predicts a deeper and narrower trough than the strain-softening model does.

The paper also discusses how to improve the modelling of the goaf behaviour. A Critical State model, i.e. the modified Cam-clay model, was implemented into the goaf. It was shown that if the goaf length is not sufficient to recover the primary stresses, the modified Cam-clay model and the double yield model predict identical goaf behaviour. Hence, it is difficult to say how much of the model discrepancies can be attributed to the goaf and how much can be attributed to the 700m of overburden. This work suggests deeper investigation of modelling the goaf behaviour by increasing the goaf length up to distance D1 and implementing more advanced constitutive models into the goaf.

ACKNOWLEDGMENTS

The authors greatly acknowledge the open fund SKLGDUEK1512 of the China University of Mining and Technology.

REFERENCES

- Badr, S., Ozbay, U., Kieffer, S. and Salamon, M. (2003). Three-dimensional strain softening modeling of deep longwall coal mine layouts. *FLAC and Numerical Modeling in Geomechanics*, 233-239. doi: 10.1201/9780203883204.ch79
- Balmer, G.A. (1952). General analytic solution for Mohr envelope. *Proceedings-American society for testing and materials*, 1260-1271.
- Bell, F. G. and Donnelly, L. J. (2006). *Mining and its Impact on the Environment*, Taylor & Francis, 547. doi: 10.2113/gsegeosci.13.3.270
- Bräuner, G. 1973. Subsidence Due to Underground Mining: Theory and practices in predicting surface deformation, *US Bureau of Mines*, 8571. doi: 10.1016/0148-9062(74)91643-x
- British Standard. (1981). *Code of Practice for Site Investigation*, 147.
- Deere, D. (1968). Geological considerations. *Rock mechanics in engineering practice*, 1-20.
- Derbin, Y., Walker, J., Wanatowski, D., and Marshall, A. (2016). Issues related to goaf modeling. *Proceedings of the 19th Southeast Asian Geotechnical Conference & 2nd AGSSEA Conference*, 1015-1021.
- Derbin, Y., Walker, J., Wanatowski., and Marshall, A. (2018). Implementation of advanced constitutive models for the prediction of surface subsidence after underground mineral extraction. Expected to be published.
- Gens, A. and Potts, D. (1988). Critical state models in computational geomechanics. *Engineering Computations*, 5, 178-197. doi: 10.1016/0148-9062(89)90209-x
- Hansen, T. H. (1988). Rock properties. *Norwegian Rock and Soil Assoc.*, 5, 41-44.
- Harrison, J. P., Hudson, J. A. and Carter, J. N. (2007). Is there a relation between the in situ principal stress magnitudes in rock masses? *Proceedings of the 1st Canada-US*

- Rock Mechanics Symposium - Rock Mechanics Meeting Society's Challenges and Demands, 675-682. doi: 10.1201/NOE0415444019-c83
- Herrero, C., Munoz, A., Catalina, J. C., Hadj-Hassen, F., Kuchenbecker, R., Spreckels, V., Juzwa, J., Bennet, S., Purvis, M., Bigby, D. and Moore, D. (2012). Prediction and monitoring of subsidence hazards above coal mines (Presidence). Luxembourg: Directorate-General for Research and Innovation, 138.
- Hoek, E. and Brown, E. T. (1980). Underground excavations in rock. Institution of Mining and Metallurgy, London, 527.
- Hoek, E. and Brown, E.T. (1997). Practical estimates of rock mass strength. *International Journal of Rock Mechanics and Mining Sciences*, 34, 1165-1186. doi: 10.1016/s0148-9062(97)00305-7
- Hoek, E. and Diederichs, M.S. (2006). Empirical estimation of rock mass modulus. *International Journal of Rock Mechanics and Mining Sciences*, 43, 203-215. doi: 10.1016/j.ijrmms.2005.06.005
- Hudson, J. A. and Harrison, J. P. (2000). *Engineering rock mechanics: an introduction to the principles*, Elsevier, 444. doi: 10.1115/1.1451165
- Indraratna, B., and Salim, W. (2002). Modelling of particle breakage of coarse aggregates incorporating strength and dilatancy. *Proceedings of the Institution of Civil Engineers*, London, 155(4): 243–252. doi:10.1680/geng.155.4.243.38691
- Itasca (2013). *Manual FLAC3D Version 5.01*.
- Lloyd, P., Mohammad, N. and Reddish, D. (1997). Surface subsidence prediction techniques for UK coalfields-an innovative numerical modelling approach. *Proceeding of the 15th Mining Congress of Turkey*, Ankara, 6-9.
- Mukherjee, C., Sheorey, P. R. and Sharma, K. G. (1994). Numerical simulation of caved goaf behaviour in longwall workings. *International Journal of Rock Mechanics and Mining Sciences & Geomechanics*, 31, 35-45. doi: 10.1016/0148-9062(94)91292-0
- Najafi, M., Jalali, S. M. E. and Khalokakaie, R. (2014). Thermal–mechanical–numerical analysis of stress distribution in the vicinity of underground coal gasification (UCG) panels. *International Journal of Coal Geology*, 134–135, 1-16. doi: 10.1016/j.coal.2014.09.014
- NCB, (1975). *National Coal Board. Subsidence Engineers' Handbook*. Mining Department, London, 111.
- Palmström, A. (1995). *A Rock Mass Characterization System for Rock Engineering Purpose*. University of Oslo, 381.
- Palmström, A. and Singh, R. (2001). The deformation modulus of rock masses—comparisons between in situ tests and indirect estimates. *Tunnelling and Underground Space Technology*, 16, 115-131. doi: 10.1016/s0886-7798(01)00038-4
- Pourhosseini, O. and Shabanimashcool, M. (2014). Development of an elasto-plastic constitutive model for intact rocks. *International Journal of Rock Mechanics and Mining Sciences*, 66, 1-12. doi: 10.1016/j.ijrmms.2013.11.010
- Salamon, M. (1983). *Rockburst hazard and the fight for its alleviation in South African gold mines. Rockbursts: prediction and control*. IMM, London, 11-36. doi: 10.1016/0148-9062(84)90579-5
- Salamon, M. (1990). Mechanism of caving in longwall coal mining. *Rock Mechanics Contributions and Challenges: Proceedings of the 31st US Symposium*, Golden,

- Colorado, 161-168.
- Shtumpf, G. G. (1994). Mechanical properties of rocks of the Kuznetsk basin and regularities of their change. *Physical-Chemical Problems of Mining*, 4, 43-51. (in Russian)
- Singh, G. S. P. and Singh, U. K. (2011). Assessment of goaf characteristics and compaction in longwall caving. *Mining Technology*, 120, 222-232. doi: 10.1179/1743286311y.0000000010
- Wilson, A.H. (1983). The stability of underground workings in the soft rocks of the coal measures. *International Journal of Mining Engineering*, 1, 91–187. doi: 10.1007/bf00880785
- Wilson, A. H. (1984). Pillar stability in longwall mining: Wilson, A H In: *State-of-the-Art of Ground Control in Longwall Mining and Mining Subsidence*, 85-95. doi: 10.1016/0148-9062(84)90575-8
- Xiao, Y., Sun, Y., Liu, H. and Yin, F. (2016). Critical state behaviors of a coarse granular soil under generalized stress conditions. *Granular Matter*, 18(2), 17. doi: 10.1007/s10035-016-0623-3
- Xu, N., Kulatilake, P.H.S. W., Tian, H., Wu, X., Nan, Y. and Wei, T. (2013). Surface subsidence prediction for the Wutong mine using a 3-D finite difference method. *Computers and Geotechnics*, 48, 134-145. doi: 10.1016/j.compgeo.2012.09.014

TABLES

**Table 1. Guidelines for the selection of the modulus ratio.
Based on Deere (1968) and Palmström and Singh (2001)**

Rock type	Class	Group	Texture				
			Coarse	Medium	Fine	Very fine	
Sedimentary	Clastic		Conglome-rates 300-400 Breccias 230-350	Sandstones 200-350	Siltstones 350-400 Greywackes 350	Claystones 200-300 Shales 150-250 ^a Marls 150-200	
	Non-clastic	Carbonates	Crystalline limestones 400-600	Sparitic limestones 600-800	Micritic limestones 800-1000	Dolomites 350-500	
		Evaporites	Gypsum (350) ^b		Anhydrite (350) ^b		
		Organic					Chalk 1000+
Metamorphic	Non-foliated		Marble 700-1000	Hornfels 400-700 Metasandstone 200-300	Quartzites 300-450		
	Slightly foliated		Migmatite 350-400	Amphibolites 400-500	Gneiss 300-750 ^a		
	Foliated ^a			Schists 250-1100 ^a	Phyllites/ Mica Schist 300-800 ^a	Slates 400-600 ^a	
Igneous	Plutonic	Light	Granite ^c 300-550 Granodiorite ^c 400-450	Diorite ^c 300-350			
		Dark	Gabbro 400-500 Norite 350-400	Dolerite 300-400			
	Hypabyssal		Porphyrics (400) ^b		Diabase 300-350	Peridotite 250-300	
	Volcanic	Lava			Rhyolite 300-500 Andesite 300-500	Dacite 350-450 Basalt 250-450	
		Pyroclastic	Agglomerate 400-600	Volcanic breccia (500) ^b	Tuff 200-400		

^a Highly anisotropic rocks: the value of MR will be significantly different if normal strain and/or loading occurs parallel (high MR) or perpendicular (low MR) to a weakness plane. Uniaxial test loading direction should be equivalent to field application.

^b No data available, estimated on the basis of geological logic.

^c Felsic Granitoids: coarse grained or altered (high MR), fined grained (low MR)

**Table 2. A Summary of Uniaxial Compressive Strength Based on Rock Type
(Palmström, 1995)**

Rock name	Uniaxial compressive strength σ_c , MPa			Rating of the factor $m_i^{1)}$	Rock name	Uniaxial compressive strength σ_c , MPa			Rating of the factor $m_i^{1)}$
	low	average	high			low	average	high	
Sedimentary rocks					Metamorphic rocks				
Anhydrite		120'?		13.2	Amphibolite	75	125	250	31.2
Coal	16"	21"	26"		Amphibolitic gneiss	95	160	230	31 ?
Claystone	2'	5'	10'	3.4	Augen gneiss	95	160	230	30 ?
Conglomerate	70	85	100	(20)	Black shale	35	70	105	
Coral chalk	3	10	18	7.2	Garnet mica schist	75	105	130	
Dolomite	60'	100'	300'	10.1	Granite gneiss	80	120	155	30 ?
Limestone	50*	100'	180*	8.4	Granulite	80'	150	280	
Mudstone	45	95	145		Gneiss	80	130	185	29.2
Shale	36"	95"	172"		Gneiss granite	65	105	140	30 ?
Sandstone	75	120	160	18.8	Greenschist	65	75	85	
Siltstone	10'	80'	180'	9.6	Greenstone	120'	170*	280*	20 ?
Tuff	3'	25'	150'		Greywacke	100	120	145	
Igneous rocks					Marble	60'	130'	230'	9.3
Andesite	75'	140'	300'	18.9	Mica gneiss	55	80	100	30 ?
Anorthosite	40	125	210		Mica quartzite	45	85	125	25 ?
Basalt	100	165	355"	(17)	Mica schist	20	80*	170*	15 ?
Diabase (dolerite)	227"	280"	319"	15.2	Mylonite	65	90	120	
Diorite	100	140	190	27 ?	Phyllite	21	50	80	13 ?
Gabbro	190	240	285	25.8	Quartz sandstone	70	120	175	
Granite	95	160	230	32.7	Quartzite	75	145	245	23.7
Granodiorite	75	105	135	20 ?	Quartzitic phyllite	45	100	155	
Monzonite	85	145	230	30 ?	Serpentinite	65	135	200	
Nepheline syenite	125	165	200		Slate	120'	190'	300'	11.4
Norite	290"	298"	326"	21.7	Talc schist	45	65	90	10 ?
Pegmatite	39	50	62						
Rhyolite		85'?		(20)					
Syenite	75	150	230	30 ?					
Ultra basic rock	80'	160	360						
Soil materials²⁾:									
Very soft clay $\sigma_c = 0.025\text{MPa}$			Soft clay $\sigma_c = 0.025 - 0.05\text{MPa}$			Firm clay $\sigma_c = 0.05 - 0.1\text{MPa}$			
Stiff clay $\sigma_c = 0.1 - 0.25\text{MPa}$			Very stiff clay $\sigma_c = 0.25 - 0.5\text{MPa}$			Hard clay $\sigma_c = > 0.5\text{MPa}$			
Silt, sand: assume $\sigma_c = 0.0001 - 0.001\text{MPa}$									
*Values found by the Technical University of Norway, (NTH) Inst. for rock mechanics.									
^Values given in Lama and Vutukuri, 1978.									
"Values given by Bieniawski, 1984.									

Table 3. Determination of m_i (Hoek and Brown, 1997)

Rock type	Class	Group	Texture			
			Coarse	Medium	Fine	Very fine
Sedimentary	Clastic		Conglomerate (22)	Sandstone 19	Siltstone 9	Claystone 4
	Non-clastic	Organic	-----Greywacke----- (18)			
			-----Chalk----- 7			
		Carbonate	-----Coal----- (8-21)			
			Breccia (20)	Sparitic Limestone (10)	Micritic Limestone 8	
Chemical		Gypstone 16	Anhydrite 13			
Metamorphic	Non-foliated		Marble 9	Hornfels (19)	Quartzite 24	
	Slightly foliated		Migmatite (30)	Amphibolite 25-31	Mylonites (6)	
	Foliated*		Gneiss 33	Schists 4-8	Phyllites (10)	Slate 9
Igneous	Light		Granite 33		Rhyolite (16)	
			Granodiorite (30)		Dacite (17)	Obsidian (19)
			Diorite (28)		Andesite 19	
	Dark		Gabbro 27	Dolerite (19)	Basalt (17)	
		Norite 22				
	Extrusive pyroclastic type		Agglomerate (20)	Breccia (18)	Tuff (15)	

*These values are for intact rock specimens tested normal to bedding or foliation. The value m_i will be significantly different if failure occurs along a weakness plane.

Table 4. Density of different geomaterial (Shtumpf, 1994)

Geomaterial type	Density, kg/cm ³
Soils	2000-2780
Sandstone	2400-2900
Siltstone	2390-2950
Mudstone	2400-2800
Distorted and coal included rock	1800-2450
Sandstone and siltstone with siderite, pyrite, chalcopryrite and with other heavy metals	2950-3600

Table 5. Subsidence factor after Bräuner (1973)

Coal field	Subsidence factor
British coal fields	0.90
Ruhr coal field, Germany	0.90
North and Pas de Calais coal field, France	0.85–0.90
Upper Silesia, Poland	0.70
Donbass district, Ukraine	0.80
Lvov-Volyn district, Ukraine	0.80–0.90
Kizelov district, Ukraine	0.40–0.80
Donetz, Kuznetsk and Karaganda districts, Russia and Ukraine	0.75–0.85
Sub-Moscow and Cheliabinski districts, Russia	0.85–0.90
Pechora, Russia	0.65–0.90
Central, USA	0.50–0.60
Western, USA	0.33–0.65

FIGURES

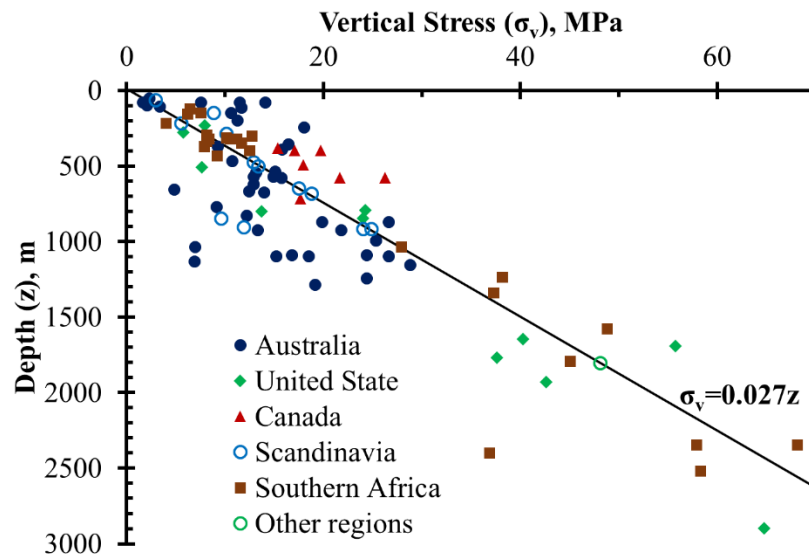


FIG. 1. Insitu vertical stress data (after Hoek and Brown (1980) in Hudson and Harris (2000))

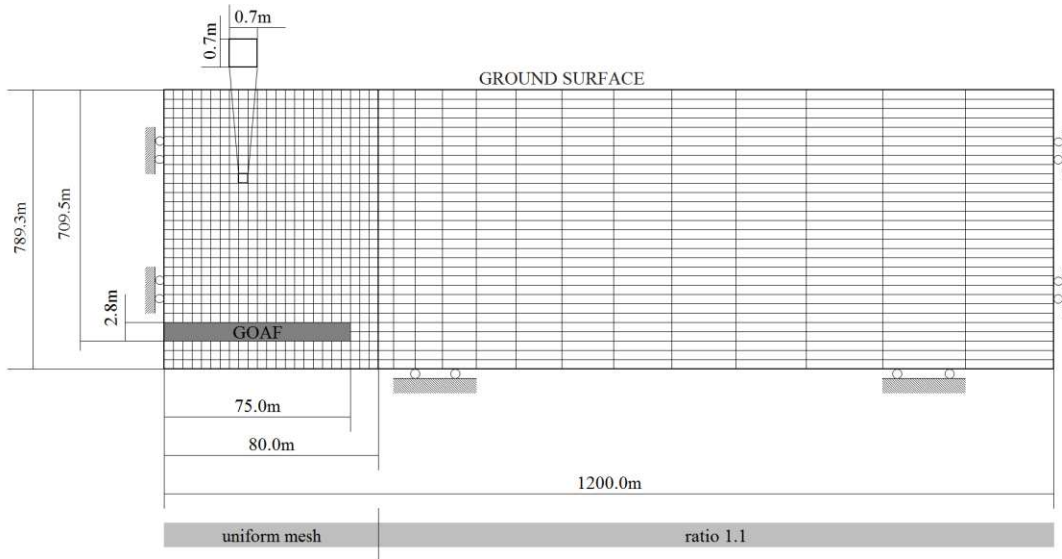


FIG. 2. Scheme of the model.

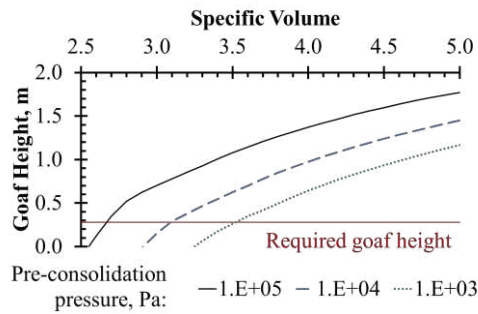


FIG. 3. Obtaining the required height of the goaf.

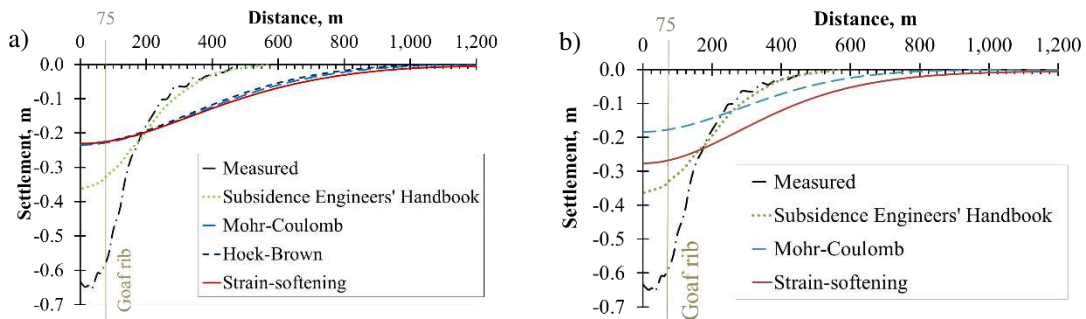


FIG. 4. Surface settlement half-profile: a) constant GSI of 40, b) increasing GSI

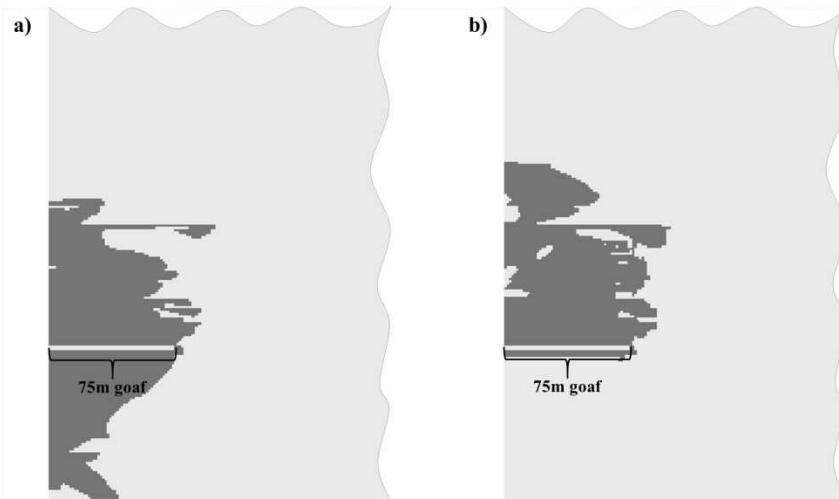


FIG. 5. Plastic deformation resulting from the excavation: a) GSI is constant with the depth; b) GSI gradually increased with the depth

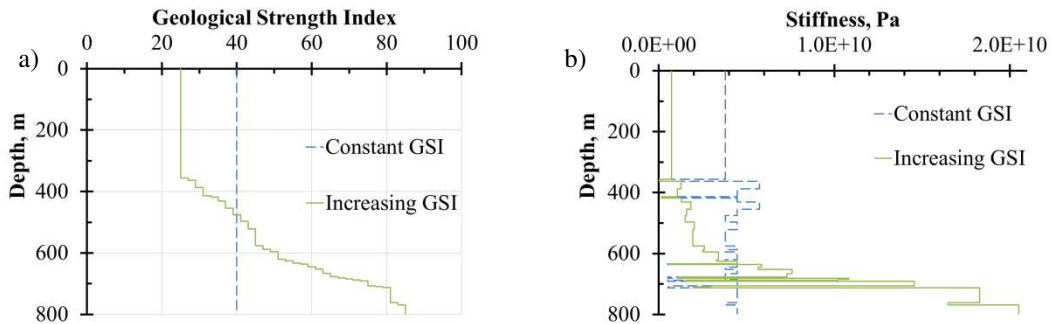


FIG. 6. a) GSI with the depth, b) stiffness vs depth

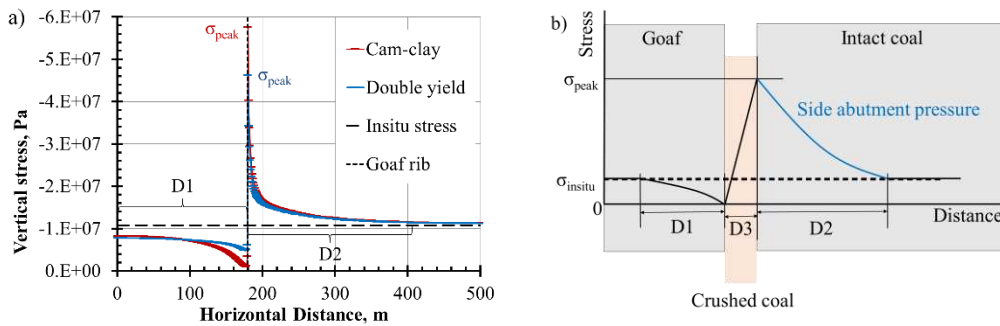


FIG. 7. Compression vertical stress within the goaf: a) fictitious model (Derbin et al., 2016) and b) theoretical (after Wilson, 1983)

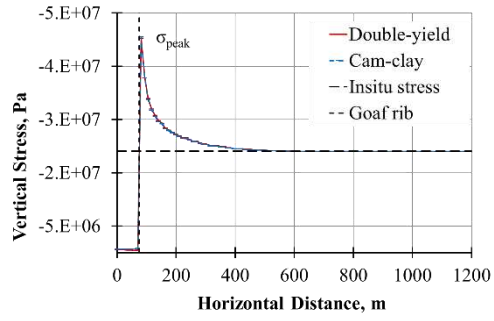


FIG. 8. Compression vertical stress within the goaf (Naburn model)